Submitted to Metallurgical
Transactions

LBL-2230
Preprint c.1

THE MECHANICAL NATURE OF STRESS-CORROSION CRACKING IN Al-Zn-Mg ALLOYS: II. ELECTROCHEMICAL-MECHANICAL MODEL

W. W. Gerberich and W. E. Wood

RECEIVED
LAWRENCE
RADIATION LABORATORY

JAN 14 1974

LIBRARY AND
DOCUMENTS SECTION

November 1973

Prepared for the U. S. Atomic Energy Commission
under Contract W-7405-ENG-48

For Reference

Not to be taken from this room

LAWRENCE BERKELEY LABORATORY
UNIVERSITY OF CALIFORNIA
BERKELEY

LBL-2230
c.1

DISCLAIMER

This document was prepared as an account of work sponsored by the United States Government. While this document is believed to contain correct information, neither the United States Government nor any agency thereof, nor the Regents of the University of California, nor any of their employees, makes any warranty, express or implied, or assumes any legal responsibility for the accuracy, completeness, or usefulness of any information, apparatus, product, or process disclosed, or represents that its use would not infringe privately owned rights. Reference herein to any specific commercial product, process, or service by its trade name, trademark, manufacturer, or otherwise, does not necessarily constitute or imply its endorsement, recommendation, or favoring by the United States Government or any agency thereof, or the Regents of the University of California. The views and opinions of authors expressed herein do not necessarily state or reflect those of the United States Government or any agency thereof or the Regents of the University of California.

The Mechanical Nature of Stress-Corrosion Cracking in Al-Zn-Mg Alloys: II. Electrochemical-Mechanical Model*

W. W. Gerberich** and W. E. Wood**

ABSTRACT

Slow crack growth during SCC of 7075 aluminum has been shown to comprise both an electrochemical and a mechanical component. These findings prompted a review of several possible mechanical models, and seven possible controlling thermally-activated processes. Since no existing interpretation could satisfy all of the observations, an empirical model was developed. The conclusion is that slight modification of many existing proposed mechanisms could explain the general features of SCC but that any theoretical model must contain some aspect of the mechanical rupture process.

---

*This research was performed at the Inorganic Materials Research Division, Lawrence Berkeley Laboratory, and Department of Materials Science and Engineering, College of Engineering, University of California, Berkeley, California 94720.

**Presently Associate Professor of Materials Science, University of Minnesota, Minneapolis, Mn 55455, and Assistant Professor, Oregon Graduate Center, Beaverton, Or. 97005, respectively.

INTRODUCTION

Stress corrosion cracking problems in high strength aluminum alloys has resulted in many investigations and almost as many questions and theories. Some of the following questions were posed a decade or more ago but still remain unanswered to a large degree:

What is the role of the PFZ?

Do the kinetics of the process mandate a combined chemical and mechanical process?

If so, what are the relative contributions of the chemical and mechanical components?

Can a single thermally-activated mechanism be associated with the SCC process in high strength aluminum alloys?

Although no one program could hope to answer all of these, recent[1] results have clearly defined the mechanical aspect of the SCC mechanism. Based on these findings several models were reviewed, however no existing interpretation could satisfy all of the observations and hence an empirical model was developed.

Thermally-Activated Nature of the Process

Before specific models are discussed, it is first useful to consider the kinetics of the growth process. Sedriks, et al.[2] have suggested that crack growth rates as rapid as 0.0002 in./min are not inconsistent with an anodic dissolution process. In a recent investigation,[1] crack growth rates as high as 0.07 in./min at 68°C and 0.006 in./min at room

temperature were observed which would tend to eliminate any mechanism dependent entirely upon anodic dissolution. However, invoking a combined chemical and rupture process allows most of the features of most mechanisms to be rationalized. The absolute magnitude of the growth rate process is not particularly illuminating in itself. Its variations with temperature does indicate something about the thermally-activated process. The apparent activation energy for the process was determined to range from 10.4 to 11.9 kcal/mol with the average value being 11.2 kcal/mole. This value was essentially independent of stress intensity factor. This is significant since it suggests that the same thermally-activated mechanism is controlling from the start to the end of the crack propagation state.

To see if this might be a true activation energy, apparent activation energy data for SCC in several aluminum alloys are presented in Table 1. It is seen that although values ranging from 10-40 kcal/mol have been reported, most of the data suggest a value of about 10-14 kcal/mol.* Part of the discrepancy is due to the different types

*After this paper was originally submitted, a recent review article by Speidel(6) came to our attention. In short transverse specimens tested under plane strain conditions, two regions of crack velocity were observed: Region I- a strongly stress-intensity dependent region with an apparent activation energy of 27 kcal/mole; Region II - a stress-intensity independent region where the apparent activation energy was 4 kcal/mol. The data in Part I of this study did not conform to either of these situations. Considering the dependence of da/dt on K^2, the relatively high K levels investigated, the essentially plane stress situation, and the large amount of ductile rupture involved, the present study should be regarded as Region III. This may not significantly alter the conclusion reached from Table 1 since either Region III of the growth process is represented here or the specimens were not short transverse. Nevertheless, it points out the necessity of determining whether Region I, II and III growth processes exhibit different apparent activation energies for all specimen orientations.

of tests and parameters utilized in measuring the activation energy. The problem with measuring total time to failure is that one mechanism (e.g. pitting) might lead to crack nucleation and another might be controlling crack propagation. Thus, for crack incubation in smooth samples, a disproportionate amount of time might be necessary at low temperatures as compared to high temperatures. As a result, the curve of log t_f vs. 1/T could be steeper than it should be if only cracking were considered and anomalously high activation energies would be measured. This effect would be least likely to manifest itself at the highest stresses where crack nucleation would be considerably easier. In fact, for Helfrich's data,[3] the highest stress level gives an activation energy (16.9 kcal/mol) that is closest to those observed by other investigators. Furthermore, one might expect that if crack nucleation by some electrochemical process is considerably easier for one condition as compared to another, as in the case of the two conditions studied by Romans and Craig,[4] then the more resistant one might be expected to give a higher apparent activation energy, as is the case. Thus, the only real anomalous result in Table 1 is the 40 kcal/mol value cited by Tromans and Pathania[5] for Al-6Zn-3Mg near 80°C. If a value of about 12kcal/mol is taken as being typical of the true activation energy, it is appropriate to consider what thermally-activated mechanisms might be responsible.

In general, several mechanisms such as anodic dissolution[7] and hydrogen diffusion,[8-9] that have already been associated with the SCC of aluminum alloys, are presented. Also, a number of mechanical mechanisms such as creep and grain boundary sliding, which might

control the plastic flow characteristics and hence be the rate-determining mechanism of the rupture process, are considered. As seen in Table 2, eight mechanisms, some of which are interrelated, are listed. Although the range of activation energies is about 10 to 80 kcal/mol, there are a cluster of activation energies in the appropriate range of 10-15 kcal/mol. Since all of these mechanisms cannot be considered in detail, a brief statement about each one will be given with some additional amplification of mechanisms II and VIII.

For Mechanism I, a dissolution rate was picked to account for almost all of the crack growth at the lowest stress intensity values, where about 80 percent of the growth appeared to be a non-rupture process. This is comparable to an exchange current density of about 1 amp/cm^2, which, in conjunction with the standard rate equation,[7] gives activation energies of about 10.3-14.4 kcal/mol. The range in activation energies was determined considering an increasing number of active dissolution sites which could be produced by either emerging dislocations, vacancies, di-vacancies, or impurity atoms, as enhanced by deformation at the crack tip.[10]

Considering mechanism II, several investigators[8-9] have suggested hydrogen involvement in the SCC process. Particularly interesting was the location of hydrogen in grain boundaries by Haynie and Boyd.[11] Autoradiographic analysis of specimens cathodically charged in a tritiated solution showed definite concentrations of hydrogen at the grain boundaries of a stressed Al-4 Zn-3 Mg specimen but not in an unstressed one. Later, Forster, et al.[12] used the same technique to indicate that

stress-induced hydrogen migration provided concentrations in slip bands during tensile deformation. Haynie and Boyd's[11] conclusion was that hydrogen may be involved in the SCC mechansim by absorbing into grain boundaries and accelerating localized attack through either a cation gradient effect or by a non-uniform distribution of protons. In either case, the presence of hydrogen might be thought of as effectively reducing the activation energy for anodic dissolution. Hence, the diffusion of hydrogen could be the thermally-activated mechanism controlling localized corrosion. Some evidence of the hydrogen effect has been obtained by Tromans and Pathania[5] who showed that crack incubation times could be decreased by a factor of two or three through a cathodic charging treatment just before the actual SCC test. However, if the hydrogen was allowed to evolve during a delay time, there was no decrease in the crack incubation time. Objections to the hydrogen mechanism have been raised[13] on the basis that various aluminum alloys may be cathodically protected even when hydrogen is evolved as a cathodic reaction product. However, a hydrogen mechanism is not necessarily inconsistent with cathodic protection. All that one has to state is that an appropriate potential for dissolution is a necessary ingredient. Given this, the hydrogen may be the rate controlling factor with respect to SCC. If the potential is too cathodic, then even though there may be a considerable amount of hydrogen present, the potential conditions for dissolution are not met and hence no SCC takes place. This was further suggested by Tromans and Pathania[5] who ran a control specimen with respect to their previous hydrogen charging experiments. They demonstrated that

cathodic charging during the SCC test retarded crack initiation and concluded that conjoint action of stress, dissolution and hydrogen were necessary for cracking to occur.

The effect discussed by Haynie and Boyd[11] is in connection with a corrosion mechansim suggested by Dignam[14] wherein the diffusivity of Al^{+++} in the oxide film could be the rate controlling process. Thus, it is possible that ionic diffusion alone could be the thermally-activated process. As shown under mechanism III, however, an activation energy of 36.8 kcal/mol is way too high unless this value can be reduced by considerably more than half through a vacancy mechanism. A similar statement is applicable to mechanism IV.

Mechanical processes such as creep (V) and atmosphere-drag control of yielding (VI) are only specualtions but could conceivably control either the dissolution part (through the production of dissolution sites) or the rupture part of the process. One interesting point is that creep of pure aluminum is controlled by a cross slip mechanism in the range of 0 to 100°C[15] while creep of an Al-3.2% Mg alloy has an anomalous rise in the activation energy near 60°C. It is thought that this large activation energy is a sum of two energies, that for cross slip and that for activation of dislocations from their atmospheres.[15] Whether or not this rise in activation energy is connected to the anomalous increase in activation energy found by Tromans and Pathania[5] at 80°C in an Al-Zn-Mg alloy is unknown. However, it is known that in Al-Mg alloys, the activation energy for the Portevin Le-Chatelier effect, which is an atmosphere-drag mechanism, is near 12 kcal/mol up to about 40°C.[16] Although atmosphere drag could not be seriously considered

in the bulk of fully aged specimens, it is possible that this could be an effect in partially aged specimens, particularly in or at the PFZ.

Considering mechanism VII, grain boundary diffusion could affect either dissolution rates or mechanical action at the grain boundary. Although activation energies for grain boundary diffusion of impurity atoms are listed in Table 2, the grain boundary self diffusion of Al would be represented by a similar value. In fact, assuming a vacancy-diffusion controlled mechanism, one obtains 14.7 kcal/mol.[17] This leads to mechanism VII where grain boundary sliding, as controlled by a vacancy-climb mechanism, might be the dominant deformation mechanism in the grain boundary region. Although most authors[18-19] have suggested that grain boundary sliding, as an effective creep mechanism, should be relegated to temperatures above 0.5 Tm, Garafalo[20] considers that it might be effective as low as 0.3 Tm. One must also consider that deformation at a crack opening is considerably different than creep under a uniform stress field. The accomodation in the matrix required to allow grain boundary sliding in a tensile specimen could be considerably greater than that required for crack propagation. In fact, one could have a very soft denuded zone opening up as the crack advances with almost no matrix deformation. It has been shown that fracture at room temperature in the absence of a corrosive environment can be associated with grain boundary shear[21] wherein the controlling mechanism might be a form of grain boundary sliding. In addition, Mullendore and Grant[22] show some evidence of room temperature grain boundary sliding in polycrystalline aluminum. Thus, if one could assume that

grain boundary sliding is the thermally activated process, a vacancy-diffusion controlled climb mechanism would give an activation energy of 14.7 kcal/mol. Evidence of a mechanically controlled process comes from some fatigue crack propagation studies by Wei[23] who indicated that the range of apparent activation energies obtained in aqueous solutions were similar to those obtained in dry gaseous environments. Clearly, some additional studies of crack growth under static load conditions on some fairly simple aluminum alloys in both aqueous solutions and dry gaseous environments are required to determine the actual thermally activated mechanism.

As a summary statement to this general discussion, it is suggested that any proposed SCC model should incorporate the following features:

(1) A crack nuclear mechanism: This could consist of a mechanical rupture at the PFZ or an electrochemical dissolution at anodic sites.

(2) A time-dependent growth process: A thermally activated process is necessary which either controls the rate of dissolution or the rate of tearing.

(3) A mechanical jump process: This actually might occur at two levels in two different ways -- a "cleavage" or ductile tearing process during the <u>slow</u> growth electrochemical stage: a "cleavage" or ductile tearing process during the stress-intensity dependent <u>rapid</u> growth stage.

In the following sections, a number of stress-corrosion-cracking models will be reviewed with respect to these features. Since it has been

clearly shown that SCC in this metal environment situation is a combined process, those models dealing exclusively with electrochemical aspects will not be emphasized.

SCC MODELS

PFZ Model

Many SCC models have been proposed[2, 24-28] which incorporate the precipitate-free zone as a dominant feature, either because of preferred dissolution or ease of mechanical rupture. In any of these, the crack growth rate may be given by

$$da/dt = f(K)\, g(T) \qquad (1)$$

The stress intensity parameter, f(K), can be rationalized in terms of either the number of anodic dissolution sites or the size of the mechanical jump, both of which would increase with increasing stress intensity. Because of the mechanical nature of the SCC process determined in a previous study,[1] the latter interpretation will be favored. The functional dependence on temperature, g(T), is a rate reaction equation which may be dependent upon hydrogen diffusion, vacancy diffusion and/or dissolution kinetics. For the time being, a phenomenological treatment will suffice and for a constant temperature g(T) is given by m. This leads to a formulation similar to

$$da/dt = m(K-K_{nucl})^2 \qquad (2)$$

except for the missing parameter, K_{nucl}. Equation (2) is the result of dead weight loaded specimens of an Al-Zn alloy tested in air[21], where m was a constant of 6×10^{-11}[psi-min]$^{-1}$, K was the applied stress intensity and K_{nucl} was the stress intensity at which cracks first started growing under a rising load test. This latter value was essentially a measure of how resistant the PFZ* was to crack nucleation. A derivation based upon plastic energy dissipation in the grain boundary region gave

$$K_{nucl} = \left(\frac{\phi}{d}\right)^{1/2} \epsilon^{*} \ell E \qquad (3)$$

where ϕ is a constant, d is the grain size, ϵ^* is the fracture strain in the grain boundary region of width, ℓ, and E is the modulus of elasticity. Considerable data for 400 and 1000 μ grain sizes supported equations (2) and (3). For clarity, just the calculated curves are shown in Fig. 1. In addition, the data of a recent investigation[1] are shown. Using an approximate value of 15,000 psi-in$^{1/2}$ for K_{ISCC} and letting $K_{ISCC} \equiv K_{nucl}$, it is seen that an identical equation to equation (2) fits the present data in Fig. 1 with the exception that m' is about m/4. One might expect growth rates in a SCC environment to be greater than those in air even though this is not the case in Fig. 1. However, the character of the precipitate and PFZ in these two cases is entirely different, e.g., Mg, Cr, Cu and Fe may allow considerable strengthening of both the PFZ and the matrix of 7075 as compared to an Al-Zn binary

*In this context, the PFZ width involved includes the whole region surrounding the precipitate plus precipitate free zone.

alloy. This is manifested in the yield strengths which were 47,500 psi for the Al-25% Zn alloy[21] and 56,800 psi for the 7075-T6 of this study. Thus, there is no a priori reason to expect these two sets of data to be completely consistent. The prominent feature is that both crack growth mechanisms may be described by the same general mechanical equation. Furthermore, the character of the dimpled rupture surfaces in the grain boundary regions of the present study are identical to those observed for the Al-25% Zn[21] fractured in air.

As discussed before, making $K_{nucl} \equiv K_{ISCC}$ gave a reasonable fit to the data of this investigation in Fig. 11. One physical interpretation of this would be that a certain stress intensity is necessary to nucleate fracture in the grain boundary region, thereby breaking the oxide film, before anodic dissolution could proceed. This is somewhat different than the models proposed by Thomas and Nutting,[24] who suggested preferred anodic dissolution at the PFZ; by Pugh and Jones[27] who suggested mechanical crack propagation in the weak PFZ; and by McEvily, et al.[28-29] who considered a film-rupture mechanism. In one way or another all three of these phenomena could be involved. The first concept could be involved as the rate determining step in controlling g(T) while the second concept could be related to the excess mechanical driving force, $(K-K_{ISCC})^2$, for crack jumps in the PFZ. Finally, the last concept could be concerned with the stress intensity to rupture the oxide film so that dissolution could proceed. Note, here, that this is considerably different than the normal film-rupture process wherein the crack propagation process is controlled solely by the thickness of the brittle

film. In the present interpretation, the film thickness would be of a negligible size compared to the actual crack movement consisting of a combined dissolution and ductile-tearing process.

The major difference between the present interpretation and the anodic dissolution interpretation is that the effect of PFZ width is considered to be a mechanical effect. After crack nucleation, the actual stress-intensity effect is probably large enough to provide sufficient mechanical energy to make the crack grow. Thus, given two specimens at the same stress intensity level with different PFZ widths, the more crack-resistant the PFZ, the more anodic dissolution necessary before mechanical growth takes place. In this way the crack growth rate and hence the time to failure could be drastically altered by the PFZ width. To see if this mechanical interpretation was viable, some results of Sedriks, et al.[26] were analyzed. They demonstrated that by increasing the PFZ width of an Al-5.3 Zn-2.5 Mg alloy from about 0.04μ to 0.35μ, they could increase the time to failure in a 3.5% NaCl environment by a factor of eight. It is shown in Appendix A that the present mechanical interpretation gives the time to failure by

$$t_f = \frac{2}{\sigma^2 \pi m} \left\{ \ln\left[\frac{K_f - K_{nucl}}{K_o - K_{nucl}}\right] - \frac{K_{nucl}}{K_f - K_{nucl}} + \frac{K_{nucl}}{K_o - K_{nucl}} \right\} \quad (4)$$

where K_o and K_f are initial and final stress intensities. It is seen that this equation has the right general form since either an increase in applied stress or a decrease in the resistance of the PFZ, i.e., a decrease in K_{nucl}, would decrease the time to failure. Also, it may be noted that if the initial stress intensity is not sufficient to nucleate a

crack in the PFZ, the solution is imaginary and if $K_o = K_{nucl}$, the failure time is infinite. This equation, along with a value of $m \approx 10^{-12} (psi^{-2} min)^{-1}$, gives the agreement shown in Fig. 2.

This unusually good agreement would normally be justification for embracing this model except that DeArdo and Townsend[30] have recently repudiated the PFZ interpretation of Sedriks et al.[26] Utilizing a similar Al-Zn-Mg alloy, they not only varied the PFZ width, but also the matrix precipitate morphology while keeping the PFZ width constant. They were thus able to demonstrate that SCC susceptibility was more a function of matrix and grain boundary precipitation rather than PFZ width. They claimed that since Sedriks, et al.[26] varied both PFZ width and matrix precipitate simultaneously, the real reason for the observed variation in failure time was the difference in matrix precipitation which affects the matrix deformation mode and hence the SCC susceptibility according to Speidel.[31] Although it is clear that such a claim is reasonable for crack incubation, it is not so clear with respect to crack propagation. As the approach considered herein is only applicable to SCC, additional tests on microstructures similar to those studied by DeArdo and Townsend should be evaluated with respect to crack propagation rates under controlled stress intensity conditions. Presently, it must be recognized that although a PFZ model can give the right trend in SCC susceptibility, this is quite possible fortuitous to a large degree.

Jacobs

Jacobs[32] assumed that crack propagation occurred by a series of chemical-mechanical steps between $MgZn_2$ particles, wherein the chemical step included anodic dissolution of the $MgZn_2$, particle and the mechanical step was of a brittle type between particles. Jacobs was right in general terms about the discontinuous nature of the SCC process, as was Dix[33] much earlier, but the details of his model do not encompass many of the present observations. Assuming for the moment that this model is correct, consider the average forward distance the crack moves. This may be assessed at two extremes: (1) where the crack takes a unit step forward involving the simultaneous fracture of all grains and (2) where cracking along each grain is independent of the other grains so that for a unit growth of the crack front, B/W subjumps are involved where W is the grain width. Although the first extreme is fairly unrealistic, it gives an excellent correspondence between the average jump distance and the spacing between $MgZn_2$ particles. For example, taking da/dt to be 2.7×10^{-5} in./sec and Δt_s to be 0.5 sec, the jump distance is 1.35×10^{-5} in. For all of the data in Table 3, the average value is about 1.32×10^{-5} in. or about 0.33μ which is very close to the spacing between $MgZn_2$ particles (0.36μ) observed in replica and transmission electron micrographs published by Jacobs.[32] However, this agreement is undoubtedly fortuitous since it would require that all growth is mechanical in nature which clearly is not the case from the fractographic evidence. Furthermore, it is difficult to rationalize the crack front moving as an entity over such a short distance. The second extreme is

thus probably a more realistic assessment. This will be discussed in more detail under the proposed model section where it is shown that the average unit step, ℓ_t, (Table 3) is probably an order of magnitude larger than the spacing between $MgZn_2$ particles. Furthermore, as seen in Table 3, the number of SWE/sec increases very rapidly with the amount of dimpled rupture observed, so that it is likely that the SWE are from the rupture regions and not the corroded regions. Thus, the SWE observed are probably not associated with discontinuous brittle fracture events but rather with discontinuous ductile rupture events. Next, several models will be considered which do include relatively large scale mechanical jumps.

Krafft-Mulherin

This model[34] assumes that there is a critical ligament size, d_T, involved in ductile fracture instability and that the condition for fracture of this ligament may be reduced by chemical attack around the periphery of the ligament. In Appendix B, the appropriate plastic flow parameters are determined and a fit to this model yields as a reasonalbe approximation that

$$da/dt \approx \frac{64V_s E[2\pi d_T]^{1/2}}{E[2\pi d_T]^{1/2} - 8K} \qquad (5)$$

where V_s is the dissolution rate or chemically-controlled attack rate. Although it is shown in Appendix B that d_T agrees very well with the average unit jump distance given in Table 3, this model can be objected to on two grounds. First, it may be shown that equation (5) gives a

$\{1/(K_{CR}-K)\}$ dependence of crack growth rate which is considerably different than the K^2 dependence observed in this investigation, and reported by Tetelman and McEvily.[35] Secondly, if the electrochemically-controlled portion of the SCC mechanism is associated with V_s, equation (5) is clearly in violation of the present study. Calculation of da/dt in terms of V_s showed that for the stress intensity range of this investigation, equation (5) would give da/dt to range from about 100 to 500 V_s. This is contrary to the present findings which indicated that the rupture and corrosion contributions were nearly equal in magnitude.

McClintock-Irwin

Whereas Krafft and Mulherin's model[34] is based upon an elastic stress distribution, McClintock and Irwin[36] have considered a fracture model based upon elastic-plastic considerations. Although little use of this has been made with respect to stress-corrosion-cracking mechanisms, Gerberich, et al. have applied it to the case of embrittlement mechanisms arising from interstitial diffusion of hydrogen[37] and carbon[38] in high strength steels. This model essentially states that there is a critical microstructural unit, ℓ^*, which fractures when the fracture ductility, ϵ^*, is exceeded within the unit. In terms of the stress intensity, this jump distance for conditions intermediate to plane strain and plane stress may be approximately given by

$$\ell^* = \frac{K^2}{2\pi\sigma_{ys}E\epsilon^*} \qquad (6)$$

If one can describe the thermally-activated mechanism to give the secondary incubation time between jumps, Δt_s, then the crack growth rate is given by

$$da/dt = \ell^*/\Delta t_s = \frac{K^2}{2\pi\sigma_{ys} E \epsilon^* \Delta t_s} \qquad (7)$$

Although this equation gives the correct K^2 dependence of growth rate, it suffers from the same deficiency as the previous model in that there is not a sufficient description of the corrosion-dependent velocity component.

Empirical Model

Rather than attempt to create a model based upon many a priori assumptions, the following treatment will only describe what has been observed experimentally and so will not define the actual mechanism. It will, however, describe the step-wise process which must be an integral part of any postulated mechanism. First, the average time it takes for the whole crack front to move one unit step will be determined; then the individual mechanical and chemical components of the unit step will be calculated; and finally the thermally-activated mechanism will be treated.

In the above discussion, it was suggested that the way in which the crack grew might be in subunits about a grain size in width. If this is the case, then for the crack to move one unit distance across the whole thickness, B/W subjumps are involved. In the SWE measurements, each

subjump is represented by a stress wave. Thus, the secondary incubation time for one unit step of the whole crack front, Δt_s^*, is given by

$$\Delta t_s^* = \Delta t_s (B/W) \qquad (8)$$

Considering that the average grain width is about 22μ, the 1540μ thick specimens would give 70 subjumps per unit step. Using equation (8) and Δt_s measurements from Table 3, results in the Δt_s^* values given in Table 3. Considering the step size, it is obvious that the total unit step, ℓ_t, is made up of chemical, ℓ_c, and mechanical, ℓ_j, components, giving

$$\ell_t = \ell_c + \ell_j \qquad (9)$$

One can separate the components by utilization of the approximation of the dimpled rupture fraction, R, estimated from the scanning electron microscopy.[1] First, it is apparent that

$$\ell_c = [(1/R)-1]\, \ell_j \qquad (10)$$

Secondly, to obtain the average value of ℓ_t, one simply multiplies the average crack growth rate by the secondary incubation time for the whole crack front giving

$$\ell_t = (da/dt)\Delta t_s^* \qquad (11)$$

Combining equations (12-14), it is seen that

$$\ell_j = R(da/dt)\Delta t_s^* \qquad (12)$$

and as a last step, ℓ_c may be obtained from equations (10) and (12). In this manner, the values of ℓ_t, ℓ_j and ℓ_c were obtained as given in Table 3. It is seen that ℓ_t is nearly equivalent to the grain size width and that ℓ_j increases with stress intensity. One final determination was an experimental estimate of the subjump width. If every SWE is associated with a subjump, then the size of this SWE should be representative of the area of ductile rupture which is ℓ_j in length. The width is simply $\Delta A/\ell_j$ which from Table 3 gives the width to range from 4.7 to 10.4μ. Within the accuracy of the experimental measurements and the applicability of the stress wave emission analysis[21] to very small jumps, it is not unreasonable to take the average jump width to be approximately a grain width (22μ). Note that this strengthens the original assumption at the start of this section.

These findings may be incorporated into a model as depicted by Fig. 3. Each subjump is represented by a chemical and mechanical part that totals a grain boundary width by a grain boundary width in area. Since the most highly stressed points are the grain-boundary triple points, it is most likely for the chemical part to start at these sites and hence there is an accentuated degree of corrosion depicted at these junctions. At low stress intensity, a relatively large amount of chemical attack precedes a relatively small ductile rupture step while the relative amounts are reversed at high stress intensities. This is logical since it is known that an increasing volume fraction of holes decreases the fracture ductility during the rupture of relatively soft materials.[39] If one wanted to invoke a critical fracture strain criteria over the whole

region, it may be shown via equation (6) that increasing the number of holes by greater chemical attack should decrease the fracture strain from 0.66 ($K = 48,300$ psi-in$^{1/2}$) to 0.18 ($K = 25,400$ psi-in$^{1/2}$). Alternatively, one could invoke a strain energy criterion such that high stress intensities. It is next appropriate to describe these experimental observations in terms of stress intensity factors so that a more quantitative treatment is possible.

First, it is necessary that no growth occurs at stress intensities less than K_{ISCC}. In terms of the applied stress intensity and K_{ISCC}, a reasonable first approximation for ℓ_c is

$$\ell_c = \frac{K_{ISCC} w}{2(K-K_{ISCC})} \tag{13}$$

Since $\ell_t \sim w$, it follows from equation (9) and (13) that

$$\ell_j = \frac{(2K-3K_{ISCC})w}{2(K-K_{ISCC})} \tag{14}$$

In Fig. 4, it is seen that equation (13) and (14) represent the data reasonably well. In the relatively small stress intensity increment where $\ell_c \sim w$, the physical significance of these equations are questionable but it will soon become apparent why these particular representations were chosen. With this rough description of ℓ_c and ℓ_j, it is next possible to consider the thermally-activated mechanism. Although the real situation is not known, a tentative assumption is that a hydrogen diffusion analysis is appropriate. Since the activation energy for this mechanism is similar to others in Table 2, this may differ from several

other approaches by only a constant. For the moment, assume that hydrogen must diffuse a distance ℓ_c to maintain the corrosion process. Furthermore, assuming some proportionality to $[Dt]^{1/2}$, it follows that

$$\ell_c = \alpha[D\Delta t_s^*]^{1/2} \qquad (15)$$

Using the second estimate of Q and D_o for hydrogen diffusion in Table 2 and the values of Δt_s^* from Table 3, it was found that a value of $\alpha = 4$ gives about a factor of two agreement with the experimental values of ℓ_c from Table 3 and the calculated values from equation (13). Physically, a constant of four could be interpreted in terms of a thin slab of hydrogen being created at the surface, wherein ℓ_c is about the furthest in a small amount of hydrogen could diffuse in a time Δt_s^*. However, besides the difficulties in depicting the physical reality of such a process,* adequate assessment of potential gradient (stress) and concentration gradient effects have not been made. Although this is possible, it is premature until greater physical evidence of a hydrogen mechanism is available. Furthermore, in keeping with the degree of accuracy represented by the other estimates, equation (15) is reasonable. With a value of four for α, combining equation (13), (14) and (15) gives

*The actual electrochemical process is more than likely a series of events within a region ℓ_c. For example, consider a number of defects in an oxide film as produced by stress concentrations at either emerging slip bands or second phase particles. These sites could act as nuclei for the reaction of aluminum with hydroxyl ions to produce hydrogen. In this case, the constant might be proportional to the square root of such sites.

$$da/dt \approx \frac{\ell_c + \ell_j}{\Delta t_s^*} \approx \left(\frac{K}{K_{ISCC}} - 1\right)^2 \frac{64 D_o e^{-Q/RT}}{w} \qquad (16)$$

It may be shown that this equation matches the data of this investigation within about a factor of two. Considering its general form, one can see that it is equivalent to equation (2) if m is taken as $64D/wK_{ISCC}^2$. In Appendix A, equation (2) was utilized to derive the time to failure in a SCC test. A similar derivation can be accomplished utilizing equation (16) which leads to

$$t_f \propto K_{ISCC}^2 \left\{ \ln \left[\frac{K_f - K_{ISCC}}{\left(\frac{K_o}{K_f}\right) K_f - K_{ISCC}} \right] - \frac{K_{ISCC}}{K_f - K_{ISCC}} + \frac{K_{ISCC}}{\left(\frac{K_o}{K_f}\right) K_f - K_{ISCC}} \right\} \qquad (17)$$

where the equation is purposely put in terms of K_{ISCC}, K_f and K_o/K_f. Taking K_f as unity, the general form of the equation is depicted in Fig. 5 for several values of K_{ISCC}/K_f. Although detailed results could not be found to substantiate the general shape of these curves with respect to aluminum alloys, such curves are found for stress-corrosion-cracking behavior of titanium alloys.[40]

In summary, the SCC mechanism at the precipitate-free-zone of aluminum alloys is an extraordinarily complicated process. No simple one parameter analysis can be generalized to explain the phenomena observed. Although phenomenological models can be derived which adequately describe the crack propagation behavior, interpretation of the actual mechanism does not necessarily follow. The present analysis has not particularly rejected the general aspects of any one theory and, in fact, some aspects of mechanical rupture models have been revitalized.

It is hoped that the present study has clarified some areas where further information is needed before more exact models of SCC behavior in aluminum alloys can be evolved.

ACKNOWLEDGEMENT

The authors wish to thank Professor E. R. Parker for his continued encouragement and advice throughout this work. This work was done under the auspices of the U. S. Atomic Energy Commission.

APPENDIX A

Dependence of Time to Failure on Precipitate Free Zone (PFZ)

The first assumption here is that the nucleation stress intensity for the first crack at a grain boundary is synonymous with the K_{ISCC} value. The second assumption is that Sedriks, Slattery and Pugh's[26] specimen configuration can be treated as an infinite plate and that a stress intensity analysis can be utilized to establish crack growth rates. Both parts of this second assumption are very marginal because the specimen section was only 1/4-inch wide and the applied stress was 80 percent of the yield strength. For initially very short cracks where $a \ll W$, the infinite plate analysis may not be too unrealistic, but the very high stress utilized makes assignment of quantitative stress intensity factors dubious at best. Nevertheless, it is instructive to derive the relationship and compare it to the data.

From the discussion in the text, it was found that the crack growth rate might be approximately given by

$$da/dt = m(K-K_{nucl})^2 \qquad \text{(A-1)}$$

For ease of integration, it is convenient to put da in terms of K. From the infinite plate solution,

$$K^2 = \sigma^2 2a \qquad \text{(A-2)}$$

and thus, for constant stress,

$$da = \frac{2KdK}{\sigma^2 \pi} \qquad \text{(A-3)}$$

Combining A-1 and A-3 and integrating, the time to failure may be obtained from

$$\int_{o}^{t_f} dt = \int_{K_o}^{K_f} \frac{2K}{\sigma^2 \pi m (K-K_{nucl})^2} \, dK \qquad \text{(A-4)}$$

This finally reduces to equation (7) in the main text. Of course, this only is valid for $K_o > K_{nucl}$, since for stress intensities less than $K_{nucl} \equiv K_{ISCC}$, there would be no crack growth. Sufficient information was not available[26] to assign good values to all of the parameters but, as an exercise, first order approximations were made. For these thin sheets tested to 80 percent of yield, a plane stress situation exists and thus K_f would be associated with the plane stress fracture toughness. A reasonable value for the alloy used by Sedriks, et al.[2], which had a considerably lower yield strength (48,000 psi) than peak-aged 7075-T6, is K_f = 70,000 psi-in.$^{1/2}$. The applied stress was 38,500 psi. Considering a half crack several grain diameters in length and a plastic zone correction, one calculates a value of K_o approaching 30,000 psi-in.$^{1/2}$. Although this value seems high, it must be emphasized that Sedriks, et al.[2] observed three stages in their stress corrosion tests. Load relaxation and dormant stages made up the bulk of the test duration while a third stage was associated with crack propagation. By the time the third stage of failure initiated, some cracking could have occurred and thus a value of K_o near 30,000 psi-in.$^{1/2}$ may not be too unrealistic. Values for K_{nucl} were calculated from equation (3). To accomplish this, an estimate of ϕ ~1500 was determined from the Al-Zn fracture data of a previous investigation.[21] This value is much

larger than that calculated from theoretical considerations and includes a multiplication factor on the PFZ width. The reason for this is that the grain boundary fracture region is not located wholly within the PFZ but extends to a considerable distance on both sides of it. A value of ϵ^* was taken as 0.30, which is typical of many aluminum alloys; the grain size, d, was 125μ or 0.005 inches; and the modulus of elasticity was 10.5×10^6 psi. These values inserted into equation (3) gives K_{nucl} for any particular PFZ size. For example, a 0.1μ PFZ gives K_{nucl} equal to 6800 psi-in.$^{1/2}$. The remaining parameter needed to calculate time to failure from equation (4) is the value of m. A value of $m \approx 10^{-12}[\text{psi}^2\text{-min}]^{-1}$ gave the best fit to data, which, as is indicated in Fig. 2 accurately represents time to failure as a function of PFZ.

One might criticize this as simply a curve fitting procedure. However, as a note in added proof, it came to our attention after this analysis was done, that Sedriks, et al.[2] had published some crack propagation data from single-edge-notch (SEN) specimens of the same material. To make a realistic comparison, the value of m should be that just associated with crack propagation. For the curve-fitting in Fig. 2, the best value of m was used to fit the total time to failure, which included both incubation, t_I, as well as propagation, t_p, times. Since, according to Sedriks, et a.,[2] $t_I \sim 3t_p$, it is realistic to use a value of m that is three times as great when just considering crack propagation. Using a value of $m \approx 3 \times 10^{-12}[\text{psi}^{-2}\text{-min}]^{-1}$ and stress intensity values calculated for the SEN configuration, the comparison of equation (A-1) to the observed crack growth rates are shown in Fig. A-1.

Since the data were obtained by differentiating the time versus crack length curves presented by Sedriks, et al.,[2] their accuracy could easily be off by a factor of two.

APPENDIX B

Krafft-Mulherin Model

Since the terminology utilized by Krafft and Mulherin is rather lengthy, the reader is referred to the original paper[34] for a detailed description. Plastic flow parameters (ϵ_T, σ_T, ϵ_E, ϵ_P, θ_T, ϵ_A, $\overline{\sigma}$, $\overline{\theta}$, and ϵ_L) were determined from a tensile stress-strain curve using the procedure outlined by Krafft and Mulherin. A plot of $\overline{\theta}/\overline{\sigma}$ versus $1/\epsilon_L$ shown in Fig. B-1 indicated that as a first approximation,

$$\overline{\theta}/\overline{\sigma} \sim \frac{E[2\pi d_T]^{1/2}}{8K} \qquad \text{(B-1)}$$

where d_T is Krafft's process zone size. At $\overline{\theta}/\overline{\sigma} = 1$, $1/\epsilon_L$ is about eight so that ϵ_{CR} is about 0.125. To derive a simple equation for the crack velocity, an approximation to the SEN specimen, which was reasonably valid for the crack length range covered in the present program, gave

$$K \sim 3\sigma[a]^{1/2} \qquad \text{(B-2)}$$

Utilizing this stress intensity approximation, a derivation for crack velocity was made assuming that the process zone size was small compared to the crack length. This gives

$$da/dt \approx \frac{8}{3} V_s \left[\frac{2\pi d_T}{a}\right]^{1/2} \left[\frac{\bar{\sigma}E}{\sigma(\bar{\theta}-\bar{\sigma})}\right] \qquad \text{(B-3)}$$

where V_s is the rate of dissolution. Equation (B-3) is essentially identical to Krafft and Mulherin's equation (5). Since d_T is supposedly an independent parameter, the value of d_T can be determined from the critical stress intensity and ϵ_{CR}. In a dry air test, K_{CR} was determined to be 51,500 psi-in.$^{1/2}$ and in conjunction with an ϵ_{CR} of 0.125, $d_T = (\frac{1}{2}\pi)(K_{CR}/\epsilon_{CR}E)^2 = 2.5\times10^{-4}$ in. or 6.3μ. Comparing this to the average forward jump distance observed at low stress intensity levels (Table 3), this is in excellent agreement. Using this value of d_T and combining equations (B-1) and (B-3), it may be shown that

$$da/dt = \frac{64 V_s E[2\pi d_T]^{1/2}}{E[2\pi d_T]^{1/2} - 8K} \approx \left\{\frac{26.4\times10^5}{4.12\times10^5 - 8K}\right\} V_s \qquad \text{(B-4)}$$

For computation purposed, E was taken as 10.5×10^6 psi, d_T was 2.5×10^{-4} in. and K is in psi-in.$^{1/2}$ units.

REFERENCES

1. W. E. Wood and W. W. Gerberich: Met. Trans., Part I of this series.
2. A. J. Sedriks, J. A. S. Green, and D. L. Novak: Met. Trans., 1, July 1970, p. 1815.
3. W. J. Helfrich: Stress Corrosion Testing, Amer. Soc. for Testing and Metals (Spec. Tech. Publ.) 425 (1967), p. 21.
4. H. B. Romans and H. L. Craig, Jr., ibid, p. 363.
5. D. Tromans and R. S. Pathania: The Electrochemical Society, Extended Abstracts, No. 62, Oct. 1969.
6. M. O. Speidel: Stress-Corrosion Cracking in High Strength Steels and in Titanium and Aluminum Alloys, Naval Research Laboratories (1972), p. 147.
7. J. M. West: Electrodeposition and Corrosion Processes, D. Van Nostrand Co., London (1965), p. 15.
8. S. Matsuo and T. Hirata: J. Japan Inst. Met., 31 No. 4 (1967), p. 590.
9. W. Eichenaner and A. Pebler: Z. Metallkunda, 48 (1957), p. 373.
10. D. A. Vermilyea: J. Electrochemical Society, 115 No. 2 (1968), p. 162.
11. F. H. Haynie and W. K. Boyd: Proc. Conf. Fundamental Aspects of Stress Corrosion Cracking, National Assn. of Corrosion Eng., Houston (1969), p. 580.
12. L. M. Foster, T. H. Jack and W. W. Hill: Met. Trans., 1 (November 1970), p. 3117.

13. D. O. Sprowls and R. H. Brown: Proc. Conf. Fundamental Aspects of Stress Corrosion Cracking, National Assn. of Corrosion Eng., Houston (1969), p. 466.

14. M. J. Dignam: J. Electrochemical Society, 109, 184, 192 (1962).

15. N. R. Borch, L. A. Shepard and J. E. Dorn: Trans. Amer. Soc. for Metals, 52 (1958) p. 494.

16. K. Mukerjee, T. May and C. D'antonio: Met. Trans., 1 No. 11 (1970) p. 3233.

17. S. H. Howe and C. Elbaum: Phil. Mag., 6 (1961), p. 1227.

18. J. E. Bird, A. K. Mukherjee and J. E. Dorn: Int. Conf. on Quant. Relation Between Properties and Microstructure, Haifa (1969).

19. T. G. Langdon: Phil. Mag., 22 No. 178 (1970) p. 689.

20. F. Garofalo: Ductility, Amer. Soc. for Metals, Metals Park, Ohio (1968) p. 87.

21. W. W. Gerberich, V. F Zackay, E. R. Parker and D. Porter: in Ultrafine-Grain Metals, ed. by J. Burk and V. Weiss, Syracuse Univ. Press, Syracuse, New York, 1970, p. 259.

22. W. Mullendore and N. J. Grant: Trans. TMS-AIME, 227 (1963) p. 319.

23. R. P. Wei: Int. J. Fract. Mech. 4 No. 2 (1968), p. 159.

24. G. Thomas and J. Nutting: J. Inst. of Metals, 88 (1959-60) pp. 81.

25. A. J. Sedriks, P. W. Slattery and E. N. Pugh: Trans. Amer. Soc. for Metals, 62 (1969), pp. 815-818.

26. A. J. Sedricks, P. W. Slattery, and E. N. Pugh: Trans. Quart. ASM, 62 No. 1 (1969), p. 238.

27. E. N. Pugh and W. P. D. Jones: Metallurgia, 63 (1961), p. 3.

28. A. J. McEvily, Jr., and A. P. Bond: On Film Rupture and SCC, Environment-Sensitive Mechanical Behavior (Gorden and Breach, New York, 1966).

29. A. J. McEvily, Jr., J. B. Clark, and A. P. Bond: Trans ASM, 60 (1967), p. 661.

30. A. J. DeArdo and R D. Townsend: Met. Trans., 1 (September 1970), p. 2573.

31. M. O. Speidel: Proc. Conf. Fundamental Aspects of Stress Corrosion Cracking, National Assn. of Corrosion Eng., Houston (1969), p. 530.

32. A. J. Jacobs: Proc. Conf. Fundamental Aspects of Stress Corrosion Cracking, National Assn. of Corrosion Eng., Houston (1969), p. 530.

33. E. H. Dix, Jr.: Trans. AIME, 137 (1940), p. 11.

34. J. M. Krafft and J H. Mulherin: Trans. Quart., ASM, 62, No. 1 (1969) p. 64.

35. A. S. Tetelman and A. J. McEvily: Fracture of Structural Materials, J. Wiley and Sons, New York (1967), p. 447.

36. F. A. McClintick and G. R. Irwin: Amer. Soc. for Testing and Mat. (Spec. Tech. Publ., 381, 1965), p. 84.

37. W. W. Geberich and C. E. Hartbower: Proc. Conf. Fundamental Aspects of Stress Corrosion Cracking, National Assn. of Corrosion Eng., Houston (1969), p. 420.

38. C. E. Hartbower, W. W. Gerberich and P. P. Crimmins: Welding J. Res. Supp., 47 (10) (1968), p. 433.

39. B. Edelson and W. Baldwin, Jr.: Trans ASM, 55 (1962), p. 230.

40. D. N. Fager and W. F. Spurr: Trans-Quarterly ASM, 61 No. 2 (June 1968), p. 283.

41. J. H. Christian and H. L. Taylor: J. Applied Phys., 38 (10)(1967).

42. F. Y. Fradin: United States Atomic Energy Report, Co-1198-486 (1967).

43. B. I. Brindley, P. J. Worthington: Acta. Met., 17 (1969), p. 1357.

44. H. B. Aaron and H. I. Aaronson: Acta Met., 16 (1968), p. 789.

45. A. Hässner: Isotopenpraxis, 5 No. 4(1969), p. 143.

Table 1. Activation energies for SCC - observed.

Investigator	Material[a]	Condition	Test Solution	Type of Test	Parameter Measured	Activation Energy kcal/mol
Tromans and Pathania[5]	Al-22Zn	-	Ethanol	Notched round tensile bars	t_1 incubation time for crack nucleation	11-12
	Al-6Zn-3Mg	-	Ethanol			11-12
	Al-6Zn-3Mg	-	3% NaCl + 2.5% K_2CrO_4			12-14[b]
	Al-6Zn-3Mg	-	3% NaCl + 2.5% K_2CrO_4			~40[c]
Romans and Craig[4]	Al-4Zn-2.8Mg (Fe-Cr-Mn-Cu)	S[d]	3.5% NaCl pH ~6	Smooth tensile and C-ring	t_f time to failure	14
	Al-4Zn-2.8Mg (Fe-Cr-Mn-Cu)	R[d]	3.5% NaCl pH ~6	C-ring		19
Helfrich[3]	AL-4.2Zn-2.5Mg (Fe-Cr-Mn-Cu)	T64	3.5% NaCl pH ~6	C-ring	t_f	16.9-20.4
Present study[1]	Al-5.6Zn-2.5Mg-1.6Cu(Cr-Fe)	T6	3.5% NaCl + $AlCl_3$, pH ~1.5	Single edge notch tensile	da/dt	10.4 - 11.9

(a) Compositions in wt. %; ( ) indicates less than one percent for each element.

(b) Temperature range 0 to 30° C.

(c) Temperature near 80° C.

(d) S temper provided low resistance to SCC and R temper provided high resistance; no other details given.

Table 2. Activation energies - possible mechanisms

Mechanism	Activation Energy Q, kcal/mol	Temperature Range Investigated, °C	Comments	References
I. Anodic Dissolution	10.3-14.4	~25	Based upon i ~1 amp/cm^2	(7)
II. Hydrogen Diffusion	11-13 10.9	570 to 630 450 to 600	D_o~0.02 cm^2/sec D_o~0.21 cm^2/sec	(8) (9)
III. Al ions in Al_2O_3	36.8	280	-	(11, 41)
IV. Bulk self-diffusion	28.7	239 to 547	-	(42)
V. Creep: in Al in Al-3.2% Mg	28 28-80	0 to 100 -30 to 120	- Peak at ~60~C	(15) (15)
VI. Serrated yielding in Al-Mg	9.7-12.9	-40 to 40	Impurity diffusion by vacancy mech.	(3, 43)
VII. Grain-boundary diffusion: Cu in Al	12.8	200 to 325	D_o~0.23 cm^2/sec measured from rate of thickening of grain boundary θ allotriomorphs.	(44)
Zn in Al	~11-17	340	Based upon D_o~ 0.2 cm^2/sec Q increased with increasing Zn	(45)
VIII. Grain-boundary sliding	14.7	>0.3T_m	Activation energy based upon vacancy diffusion (17) in the grain boundary.	(18-20)

Table 3. Stress-wave and fractographic observations.

K_{Ave}, psi-in.$^{1/2}$	T, °C	SWE/sec	Δt_s, sec	Dimple Rupture, %
25,400	23	2.0	0.5	20
36,200	33	6.6	0.151	33
48,300	23	11.0	0.091	80

K_{Ave}, psi-in.$^{1/2}$	da/dt, in./sec$\times 10^5$	SWE Amplitude, g, ft/sec$^2\times 10^4$, ΔA, in.$^2\times 10^6$	
25,400	2.7	2.3	0.078
36,200	10	3.6	0.085
48,300	12	5.7	0.113

K_{Ave} psi-in.$^{1/2}$	Δt_s^* sec.	ℓ_t in.$\times 10^4$(μ)	ℓ_c in.$\times 10^4$(μ)	ℓ_j in.$\times 10^4$(μ)	$\Delta A/\ell_j$ in.$\times 10^4$(μ)
25,400	35	9.45 (24)	7.56 (19.2)	1.89 (4.8)	4.1 (10.4)
36,200	10.7	10.68 (27)	7.12 (18)	3.56 (9.0)	2.4 (6.1)
48,300	6.4	7.62 (19.4)	1.52 (3.9)	6.10 (15.5)	1.9 (4.7)

Figure Captions

Fig. 1 Stress corrosion crack growth rate vs applied stress intensity.

Fig. 2 Time to failure vs the precipitate free zone width.

Fig. 3 Model showing the two component nature of SCC for both low and high applied stress intensities. ℓ_c represents the segment of crack growth associated with electrochemical dissolution, and ℓ_t represents a single increment of crack growth which comprises both ℓ_c and ℓ_j.

Fig. 4 Crack movement vs applied stress intensity for the individual and combined components of crack growth. ℓ_j = mechanical movement, ℓ_c = electrochemical movement.

Fig. 5 The effect of the ratio of the initial stress intensity, K_o, to the plane stress fracture toughness, K_f, on the time to failure predicted by equation 20 in the text.

Fig. A-1 Stress corrosion crack growth rate vs applied stress intensity for different precipitate free zone widths.

Fig. B-1 The ratio of the slope of the true stress-true strain curve, $\bar{\theta}$ to the true stress, σ, vs the longitudinal strain, ϵ_L. (After the Krafft-Mulherin model[8]).

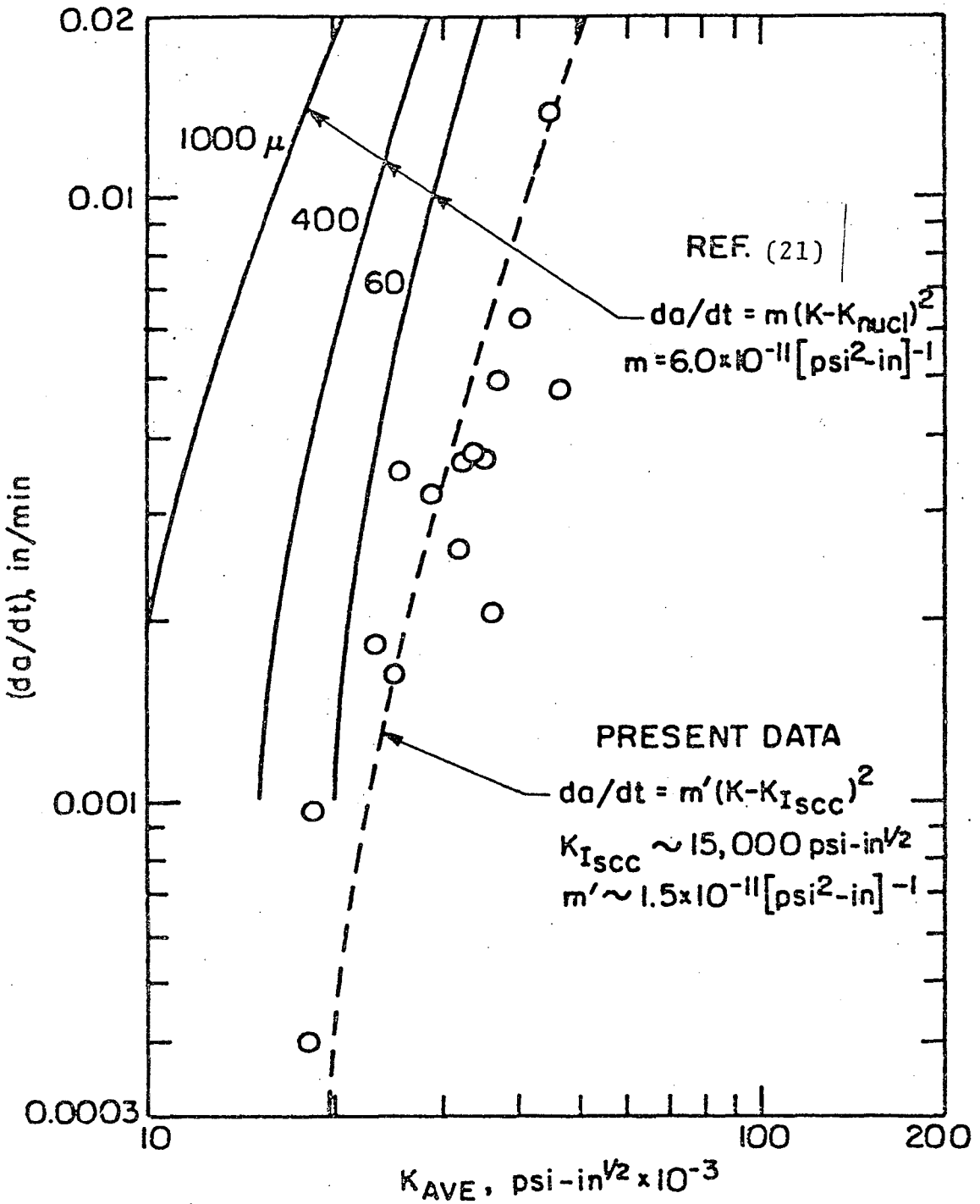

XBL 721-5914

Fig. 1

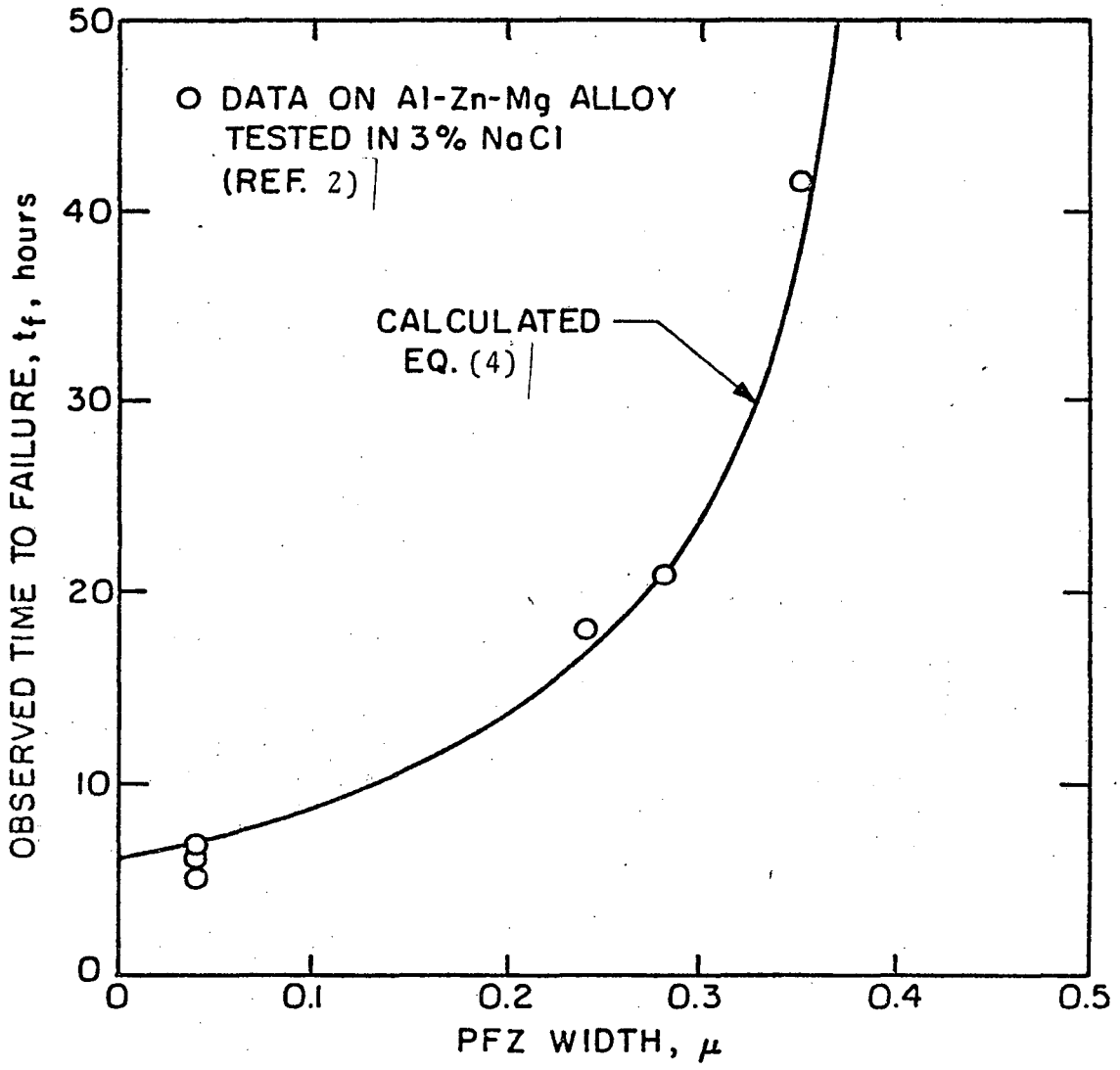

XBL 721-5915

Fig. 2

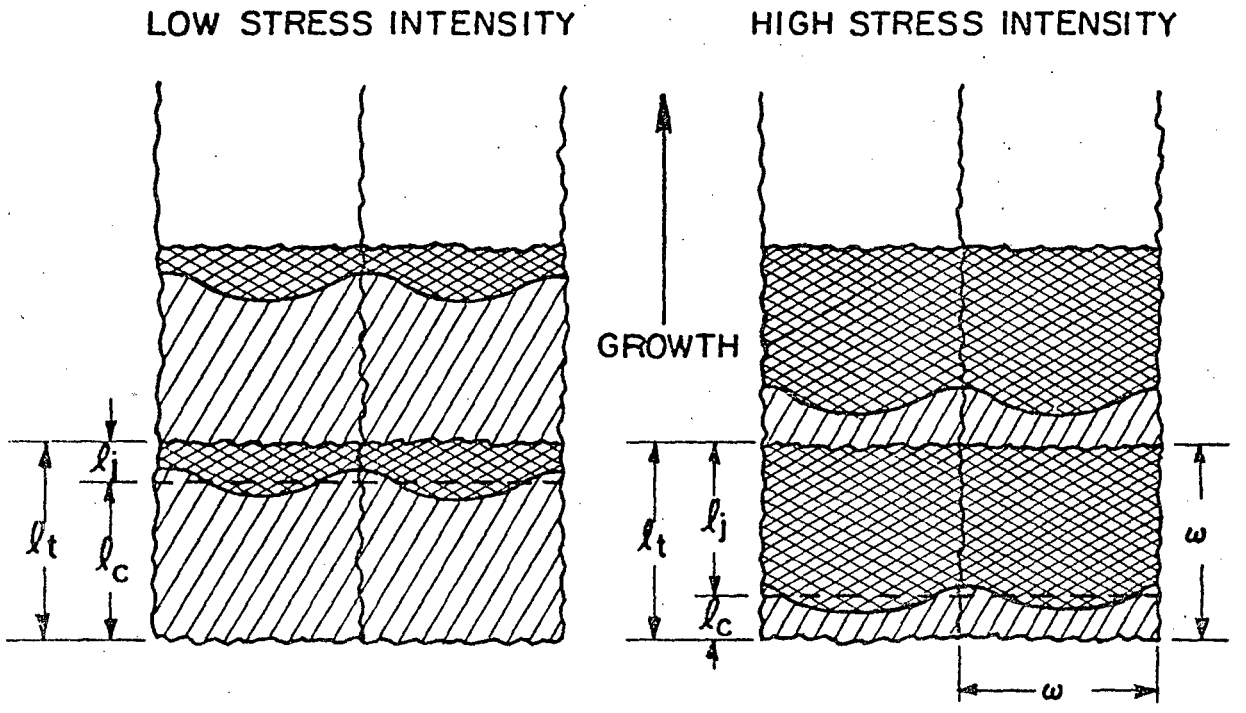

XBL 721-5916

Fig. 3

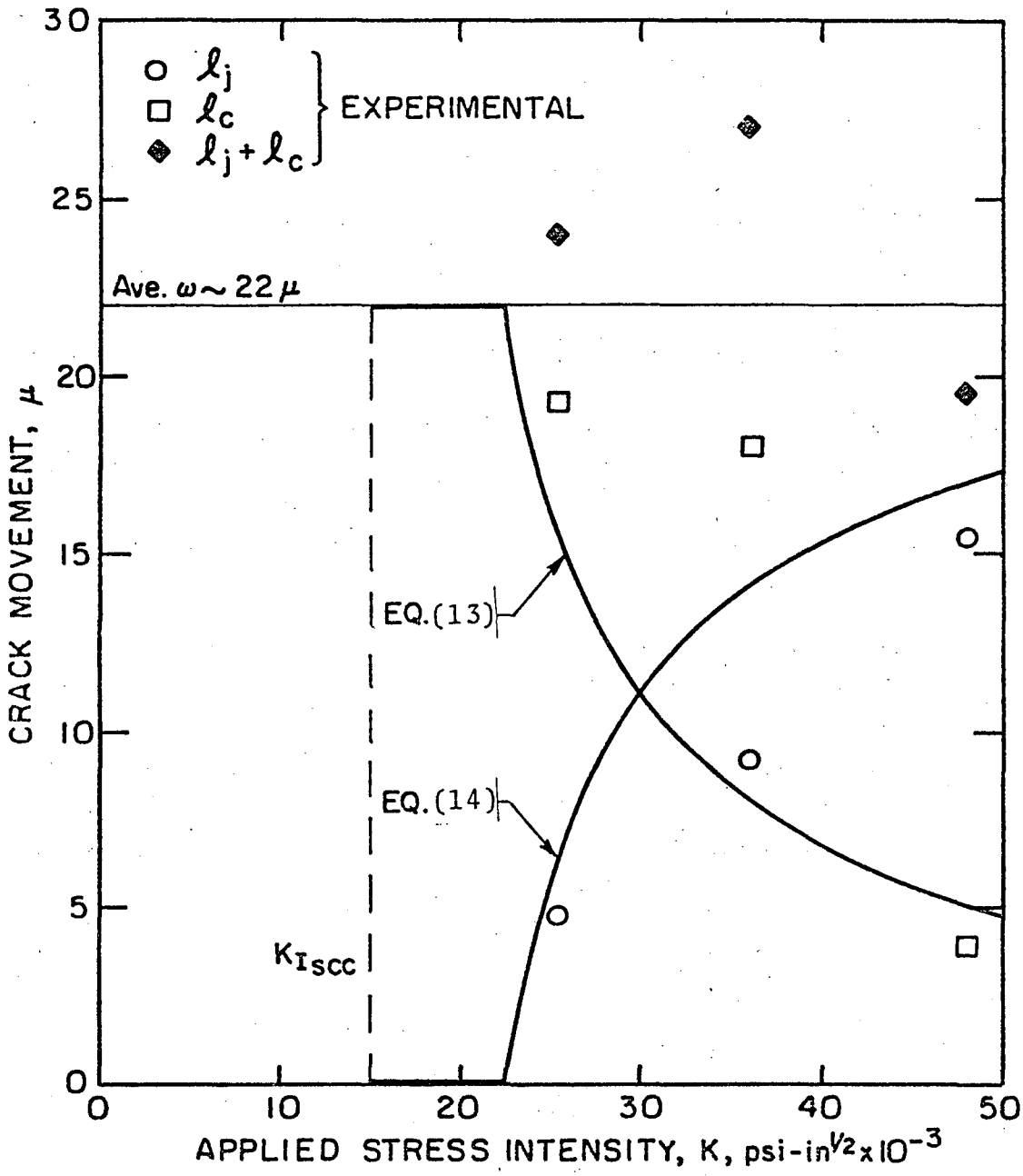

XBL 721-5917

Fig. 4

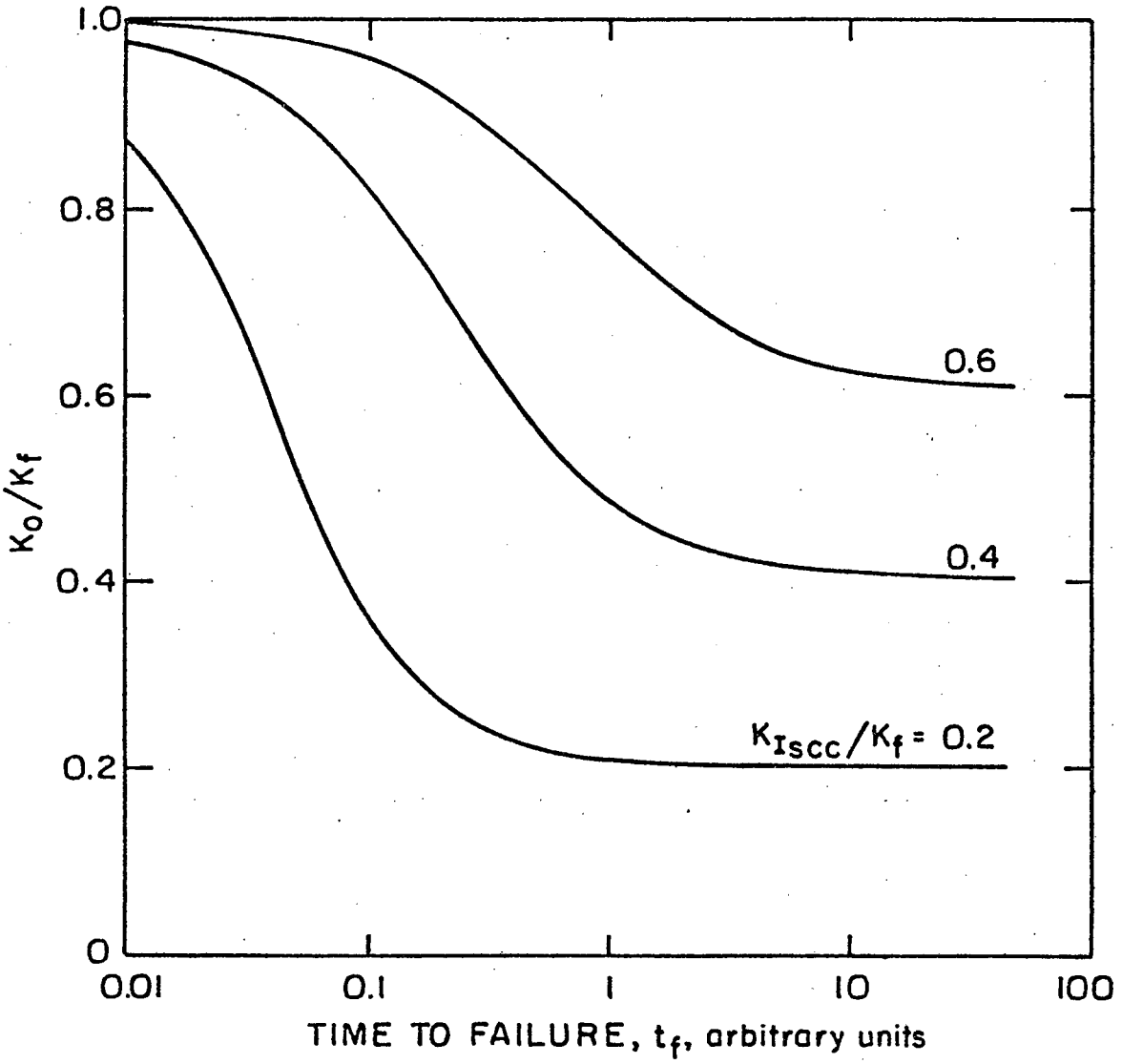

XBL 721-5918

Fig. 5

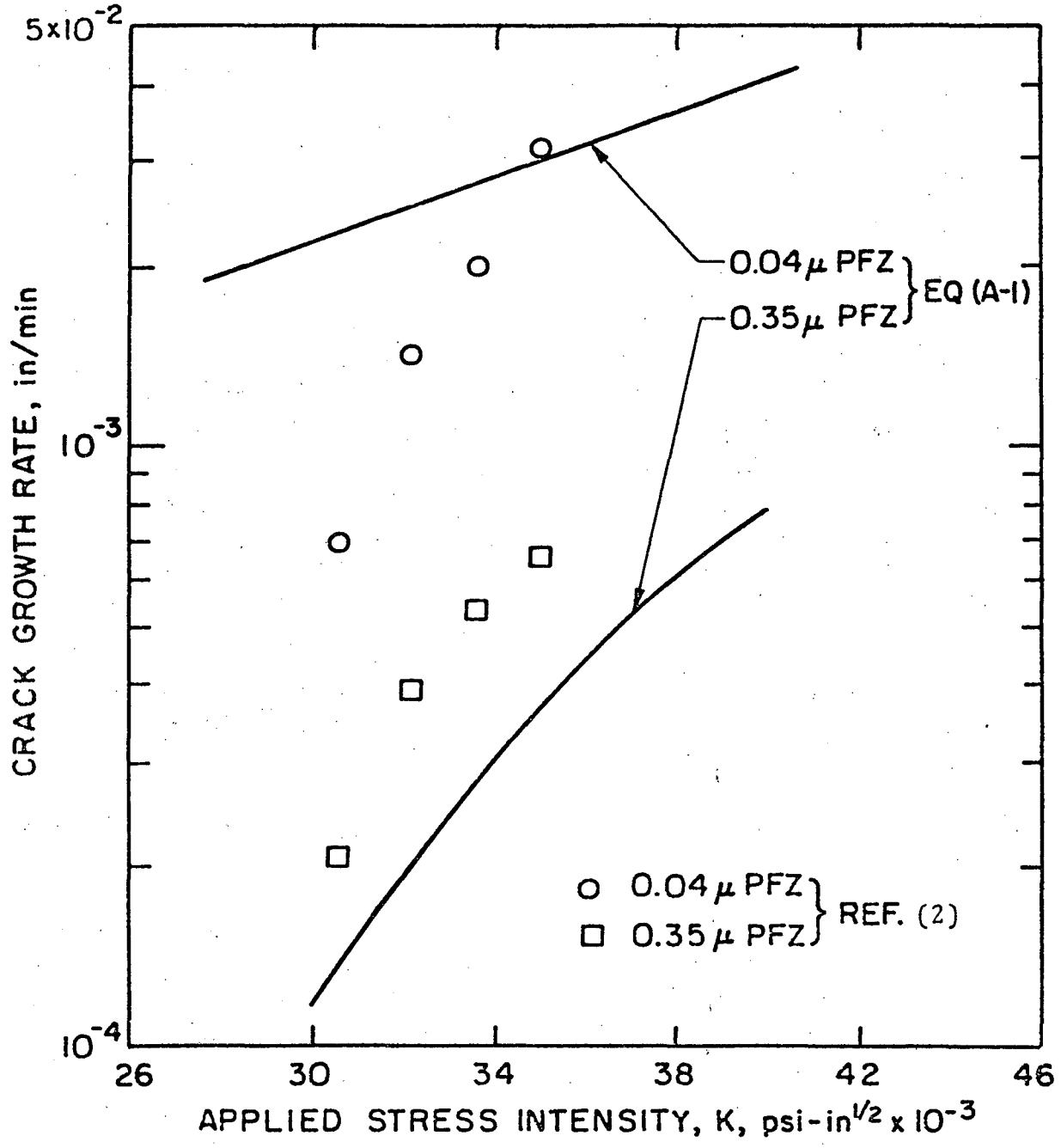

XBL 721-5919

Fig. A-1

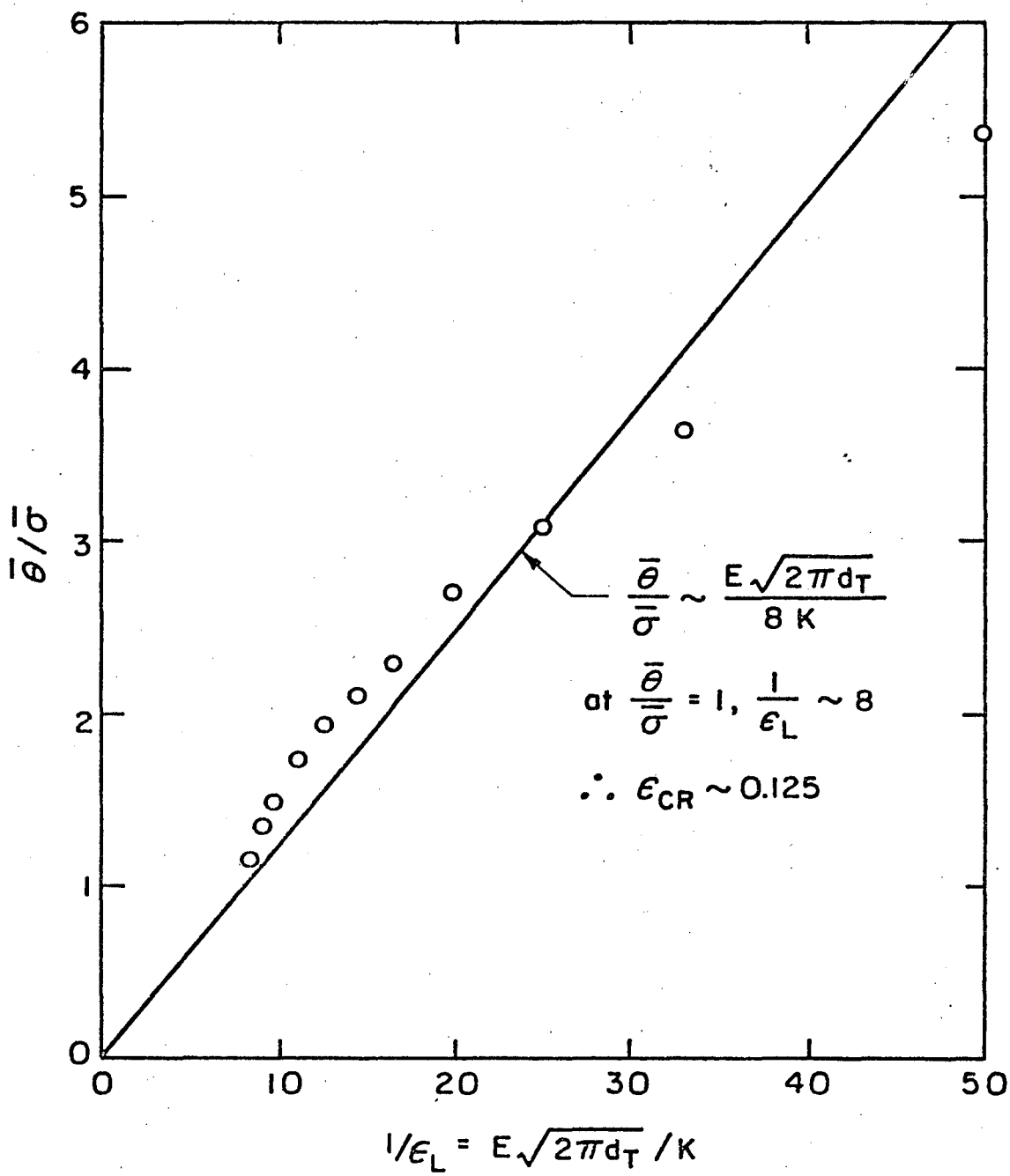

XBL 721-5920

Fig. B-1

LEGAL NOTICE

This report was prepared as an account of work sponsored by the United States Government. Neither the United States nor the United States Atomic Energy Commission, nor any of their employees, nor any of their contractors, subcontractors, or their employees, makes any warranty, express or implied, or assumes any legal liability or responsibility for the accuracy, completeness or usefulness of any information, apparatus, product or process disclosed, or represents that its use would not infringe privately owned rights.

TECHNICAL INFORMATION DIVISION
LAWRENCE BERKELEY LABORATORY
UNIVERSITY OF CALIFORNIA
BERKELEY, CALIFORNIA 94720